# Integration of multi-objective reliability-based design optimization into thermal energy management: Application on phase change material-based heat sinks

B. Debich, A. Yaich, K. Dammak, A. El Hami, W. Gafsi, L. Walha, M. Haddar

# Integration of multi-objective reliability-based design optimization into thermal energy management: Application on phase change material-based heat sinks

B. Debich[a,b,*], A. Yaich[c], K. Dammak[a], A. El Hami[a], W. Gafsi[b], L. Walha[b], M. Haddar[b]

[a] *Laboratory of Mechanics of Normandy (LMN), INSA Rouen, University of Rouen, 76801, St Etienne de Rouvray, France*
[b] *Mechanical Modeling and Manufacturing Laboratory (LA2MP), National School of Engineers of Sfax, University of Sfax, 3038, Sfax, Tunisia*
[c] *Institut Clement Ader(ICA), Universite de Toulouse, CNRS/INSA/ISAE/Mines Albi/UPS, Toulouse, France*

## Abstract

Phase change material-based heat sinks are widely used in several industrial applications such as in the field of industrial automation and mechatronics. Nowadays, several researchers aim to obtain an optimal design of these systems in order to ameliorate its performances. Nevertheless, uncertainties are not considered for the majority of these studies. Furthermore, it has been confirmed that deterministic multi-objective optimization (DMOO) may lead to an unreliable design. In this study, a new methodology that leads to perform the Multi-Objective Reliability-Based Design Optimization (MORBDO) for thermal management of a passive cooling system is proposed. It consists in coupling the Finite Element Model (FEM), MORBDO procedures and surrogate approaches. Kriging predictor is used to construct metamodels and then validated using Cross-Validation (CV) and error predictions. A numerical investigation is carried out to study the different DMOO and MORBDO approaches. In this study, a 3D PCM-based round pin-fin heat sink is detailed. The aim of this problem is to minimize two objective functions: the cost (total volume $V$) and the final cooling time $t_f$ by considering both thermal and physical constraints. For this purpose, geometrical uncertain parameters are considered such as length $L$, height $H$ and $\phi$ pin diameter of the heat sink. This study leads to develop a well-distributed reliable Pareto solutions by combining the Robust Hybrid Method (RHM) and the Constrained Non-dominated Sorting Genetic Algorithm (C-NSGA-II). Then, the efficiency of the proposed MORBDO-RHM approach for PCM-based heat sink is verified.

*Keywords:* Thermal energy management; PCM-based heat sinks; Kriging approach; Pareto optimal front; C-NSGA-II; MORBDO-RHM.

*Corresponding author
*Email address:* bessem.debich@insa-rouen.fr (B. Debich)

**Nomenclature**

**Abbreviations**

| | |
|---|---|
| ANN | Artificial neural networks |
| Cov | Covariance |
| CV | Cross-validation |
| DDO | Deterministic design optimization |
| DOE | Design of experiments |
| FES | Finite element simulation |
| HDS | Hybrid design space |
| HM | Hybrid method |
| HS | Heat sink |
| HSU | Heat storage unit |
| LHS | Latin hypercube sampling |
| MAE | Maximum absolute error |
| MCS | Monte Carlo simulation |
| MHM | Modified hybrid method |
| MSE | Mean squares error |
| PCM | Phase change material |
| QRS | Quadratic response surface |
| RBDO | Reliability-based design optimization |
| RHM | Robust hybrid method |
| RME | Relative mean error |
| RMSE | Root mean squared error |
| RSM | Response surface methodology |
| SPTs | Set point temperatures |
| TM | Thermal management |

**Symbols**

| | |
|---|---|
| $\hat{y}(\mathbf{x})$ | The predictor of the model |
| $\mathbf{F}$ | Model matrix |
| $\mathbf{f}(\mathbf{x})$ | Vector of regression basis function |
| $\mathbf{K}$ | Matrix of correlation functions |
| $\mathbf{r}(\mathbf{x})$ | Vector of correlation functions |
| $\mathbf{x}$ | Design variables vector |
| $\mathbf{x}_s$ | Set of samples |
| $\mathbf{y}_s$ | Responses of the sample set |
| $A_m$ | Mushy region |
| $C_p$ | Specific heat of fusion |
| $f(x)$ | Objective function |
| $g$ | Gravitational acceleration |
| $G_i(x,y)$ | Performance functions |
| $H$ | Height of heat sink |
| $H$ | Total enthalpy of PCM |
| $h_s$ | Specific enthalpy |
| $h_j(x)$ | Deterministic constraints |
| $h_{s,ref}$ | Referential enthalpy |
| $L$ | lenght of heat sink |
| $L_f$ | Laten heat of fusion |
| $lb$ | Lower bound |
| $m$ | Dimensional problem |
| $n$ | Number of design points |
| $P$ | Pressure |
| $p$ | Number of kriging coefficients |
| $P_i^T$ | Target failure probability |
| $Pr[.]$ | Probability operator |
| $S$ | Source term |
| $S_g$ | Global safety factor |
| $S_h$ | Energy source term |
| $T$ | Temperature |
| $t$ | Time |
| $T_l$ | Liquid temperature |
| $T_s$ | Solid temperature |
| $T_{amb}$ | Ambient temperature |
| $T_{max}$ | Maximum temperature |
| $T_{ref}$ | Referential temperature |
| $u, v, w$ | Velocity components in $x$, $y$ and $z$ directions |
| $ub$ | Upper bound |
| $V$ | Volume |
| $x$ | Deterministic design variables |
| $x^*$ | Optimal point |
| $y$ | Random variables |
| $y^*$ | Failure point |
| $Z(\mathbf{x})$ | Stochastic process |

**Greek symbols**

| | |
|---|---|
| $\alpha_w$ | Thermal expansion coefficient |
| $\beta_t$ | Target reliability level |
| $\boldsymbol{\beta}$ | Vector of regression coefficients |
| $\boldsymbol{\theta}$ | Vector of the correlation function parameters |
| $\Delta H$ | Latent heat |
| $\lambda$ | Thermal conductivity |
| $\mu$ | Dynamic viscosity |
| $\phi$ | Pin fin diameter |
| $\rho$ | Density |
| $\sigma^2$ | Variance of the stochastic model |
| $\varepsilon$ | Normal random error |
| $\xi$ | Liquid fraction of PCM |
| $d_\beta(x,y)$ | Distance between the optimal and design points |
| $L(\boldsymbol{\beta}, \sigma^2, \boldsymbol{\theta})$ | Likelihood function |

## 1. Introduction

In recent years, thermal management in the field of mechatronics has become an important factor for researchers in electronic packages design. In this context, electronic components are getting ever-smaller with more design features in size due to the development of modern technologies of electronic equipment. In fact, a high power and performance dissipated by the electronic component can lead, not only to reduce their lifetime, but also to its immediate failure. To this end, an efficient and novel cooling technology is needed to overcome the overheating phenomenon and to avoid the deterioration of the device. Furthermore, the choice of such a cooling system is based on many factors such as material cost, heat dissipation rate, maintenance and space [1].

In the literature, several technics of passive cooling are developed to ensure the smooth operation of electronic devices using PCM-based heat sinks [2–4]. However, standard cooling methods would not be sufficient. Therefore, to improve the performance of passive cooling electronic device technologies, many studies are developed and some of them are based on Phase Change Materials (PCM) [5, 6]. An experimental study is investigated in [7], to improve and ensure the reliability and functionality of the installed features. A parametric study leads to improve the thermal performance of PCM-based heat sinks by changing the PCM volume fraction and pin thickness at various heat fluxes. A numerical and experimental studies are presented by Thomas et al. [8] in order to evaluate the thermal performance of a PCM-based heat sink using n-Eicosane at many constant input power levels. In this study, the effect of natural convection has been discussed. Nowadays, PCM-based heat sink optimization presents a huge challenge for developers. A numerical study is presented in [9] which an optimal model is proposed in a passive cooling application using PCM-based plate fin matrix for charging and discharging phases. The main purpose of this study is to improve the thermal performance of the heat storage unit (HSU) by changing the input power level, PCM material, PCM volume fraction and heat sink geometry.

Integration of reliability methods in the optimization algorithm presents a new challenge in mechatronics problem. The Reliability-Based Design Optimization (RBDO) aims then to find the best compromise between cost and safety [10]. In this context, an efficient RBDO study for PCM-based heat-sink is presented in [11, 12]. These studies lead to determine an optimal and reliable design of a cooling system where two-dimensional Finite Element Simulations (FES) are performed. These studies prove that, Deterministic Design Optimization (DDO) approach leads to determine an optimal solution, but it represents a missing level of confidence and a significant risk of failure, due to non-considering uncertainties. Hence, to overcome this issue, it is recommended to integrate, during the optimization process, the reliability analysis. Using the classical RBDO approach and, to obtain optimal results, coupling of physical space and normalized space is needed. Which means a high computation time for such an optimization problem [13–15]. In order to overcome this issue, Kharmanda et al. [16] proposed a novel RBDO methodology called Hybrid reliability-optimization Method (HM) where its efficiency is presented and discussed. This method

efficiently reduces the computing time comparing with the classical approach. However, the optimization problem becomes more complex and then it can lead to an infeasible solution. In order to solve the difficulties of the classical one, Yaich et al. [17] proposed a novel methodology called Robust Hybrid Method (RHM). The efficiency of this method has been verified only on static and some specific nonlinear cases such as fatigue damage [17], coupled acoustic-structural system [18, 19] and shape memory alloy micro-pump [20]. In addition, in [21, 22], the authors aim to develop a new approach applied to an offshore wind turbine, which it called Modified Hybrid Method (MHM) in order to avoid issues of other RBDO methods.

Otherwise, such an RBDO method needs a large number of evaluations. In the case of PCM-based heat sink, a non-linear transient 3D model analysis is expensive in term of computational time. To this end, surrogate models are then recommended as an alternative to define original models' approximations. It consists in constructing mathematical models, to determine the link between inputs and outputs of a specified system [23, 24]. Recent approaches are developed in the field of design optimization [25] and probabilistic analysis [26, 27], using surrogate models. Response Surface Methodology (RSM), Artificial Neural Networks (ANN), Radial Basis Function (RBF) method and Kriging method are the most popular surrogate modelling used recently. In [28], metamodels are applied in the field of mechanical manufacturing for the purpose to enhance the computational efficiency. Also, Fatma et al. [29] studied many metamodel techniques for a NiTi micro actuator. A Monte Carlo Simulations (MCS) are then performed in order to prove its efficiency, using the constructed metamodel. These studies demonstrate that kriging method presents more efficiently and gives the best approximation of the original model. Recently, Dammak and El Hami [30, 31] studied a numerical application of a cementless hip prosthesis and a coupled acoustic-structural system. These studies are based on coupling multi-objective optimization problem (MORBDO) with surrogate models. It has been demonstrated that the studied problem using Kriging approach has the ability to generate a well-distributed reliable Pareto solution.

The aim of this paper is to propose a new methodology that leads to determine an optimal design of a PCM-based round pin-fin heat sink with a required reliability level. Both deterministic and multi-objective reliability optimization are presented. For this purpose, the Constrained Non-dominated Sorting Genetic Algorithm (C-NSGA-II) is coupled with HM and RHM approaches respectively. DMOO and MORBDO models are next coupled with surrogate models which considerably reduced the computing time. To present the advantages of the proposed method, a detailed numerical application of PCM-based round pin-fin heat sink is investigated. Results show the improvement of the resulting optimal solution using MORBDO-RHM coupled with Kriging surrogate model, and its capability to develop a well-distributed reliable Pareto solutions with a required reliability level.

## 2. Heat transfer and PCM behavior: Mathematical model

The heat generated by the input power is transferred to all surfaces of heat sink by conduction. In fact, PCM allows energy to be absorbed by changing from the solid state to the liquid state. The dissipated energy by the PCM causes its transformation from liquid to solid state. It is supposed that thermo-physical properties of the PCM are independent of temperature and only the conduction equation is taken into consideration for the aluminum section as presented in equation (1):

- **Energy conservation**:

$$\rho C_p(\frac{\partial T}{\partial t} + u\frac{\partial T}{\partial x} + v\frac{\partial T}{\partial y} + w\frac{\partial T}{\partial z}) = \lambda(\frac{\partial^2 T}{\partial x^2} + \frac{\partial^2 T}{\partial y^2} + \frac{\partial^2 T}{\partial z^2}) + S_h \tag{1}$$

Where, $\rho$, $C_p$ and $\lambda$ are respectively the density, specific heat of fusion and thermal conductivity of aluminum.
The latent heat storage is presented by the energy source term $S_h$ due to melting and it is presented as follow:

$$S_h = -\frac{\partial}{\partial t}(\rho \Delta H) \tag{2}$$

The total enthalpy of PCM can be calculated as the sum of the latent heat $\Delta H$ and the specific enthalpy $h_s$:

$$H = \Delta H + h_s \tag{3}$$

As mentioned in equation (3), the specific enthalpy $h_s$ can be defined as follows:

$$h_s = \int_{T_{ref}}^{T} C_p \, dT + h_{s,ref} \tag{4}$$

Additionaly, the latent heat $\Delta H$ is calculated as follows:

$$\Delta H = \xi L_f \tag{5}$$

As mentioned in equation (5), $L_f$ and $\xi$ refer to latent heat of fusion and liquid fraction of PCM respectively. In fact, the parameter $\xi$ presents the liquid quantity relative to the total volume of PCM and can be defined as below:

$$\xi = \begin{cases} 0 & \text{if } T \leq T_s \\ \frac{T-T_s}{T_l-T_s} & \text{if } T_s < T < T_l \\ 1 & \text{if } T \geq T_l \end{cases} \tag{6}$$

According to equations (3) to (5), the total enthalpy of PCM $H$ can be calculated by:

$$H = \int_{T_{ref}}^{T} C_p \, dT + h_{s,ref} + \xi L_f \tag{7}$$

The governing equations of mass and momentum conservation are defined as follow:

- **Mass conservation**:

$$\frac{\partial \rho}{\partial t} + \frac{\partial(\rho u)}{\partial x} + \frac{\partial(\rho v)}{\partial y} + \frac{\partial(\rho w)}{\partial z} = 0 \tag{8}$$

Note that $u$, $v$ and $w$ present velocity components in $x$, $y$ and $z$ directions, respectively. Furthermore, it is considered that the PCM in the liquid phase is an incompressible Newtonian fluid the fact that the density of the PCM is considered unchangeable for any fluid particle ($\frac{\partial \rho}{\partial t} = 0$). So, the previous equation is reduced to:

$$\frac{\partial(\rho u)}{\partial x} + \frac{\partial(\rho v)}{\partial y} + \frac{\partial(\rho w)}{\partial z} = 0 \tag{9}$$

- **Momentum conservation**:

$$\rho(\frac{\partial u}{\partial t} + \frac{\partial(u^2)}{\partial x} + \frac{\partial(uv)}{\partial y} + \frac{\partial(uw)}{\partial z}) = -\frac{\partial P}{\partial x} + \mu[\frac{\partial^2 u}{\partial x^2} + \frac{\partial^2 u}{\partial y^2} + \frac{\partial^2 u}{\partial z^2}] + S.u \tag{10}$$

$$\rho(\frac{\partial v}{\partial t} + \frac{\partial(uv)}{\partial x} + \frac{\partial(v^2)}{\partial y} + \frac{\partial(vw)}{\partial z}) = -\frac{\partial P}{\partial y} + \mu[\frac{\partial^2 v}{\partial x^2} + \frac{\partial^2 v}{\partial y^2} + \frac{\partial^2 v}{\partial z^2}] + S.v \tag{11}$$

$$\rho(\frac{\partial w}{\partial t} + \frac{\partial(uw)}{\partial x} + \frac{\partial(vw)}{\partial y} + \frac{\partial(w^2)}{\partial z}) = -\frac{\partial P}{\partial z} + \mu[\frac{\partial^2 w}{\partial x^2} + \frac{\partial^2 w}{\partial y^2} + \frac{\partial^2 w}{\partial z^2}] - \rho g \alpha_w (T - T_s) + S.w \tag{12}$$

Where, $\mu$ presents the dynamic viscosity, $\alpha_w$ is the thermal expansion coefficient, $P$ is the pressure and $g$ is the gravitational acceleration. Due to the gravitational acceleration direction (negative $z$-direction), the Boussinesq approximation is determined by adding $\rho g \alpha_w (T - T_s)$ term as presented in equation (12).
The following equation presents the source term $S$:

$$S = \frac{(1-\xi)^2}{(\xi^3 + \varepsilon)} A_m \tag{13}$$

To avoid division by zero in equation (13), a small positive parameter $\varepsilon$ is used ($\varepsilon = 10^{-10}$). The constant $A_m$ presents the consecutive number in the mushy region and it is recommended to take $A_m = 10^5$ in several studies [32–34].
Mathematical models in this study can be founded in Wang and Yang [32, 33], Shatikian et al. [34] and Nayak et al. [35]. They evaluated the performance of thermal management based on PCM in internal fins.

## 3. Surrogate models

### *3.1. Description of surrogate modeling process*

Recently, metamodels are widely used in current engineering analysis in order to reduce the calculation cost. Surrogate models aim to construct the mathematical approximations

to estimate system behaviour and to define the relationship between inputs and outputs of the system [24]. The most used surrogate modelling methods are Radial Basis Function (RBF) method, Response Surface Methodology (RSM), Artificial Neural Networks (ANN) and Kriging method [23, 24]. Several researches [28–30] demonstrate that the Kriging approach leads to a best approximation to a finite element analysis particularly for non-linear problems. In this study, Kriging metamodel method is used to evaluate the outputs of PCM-based heat sink in order to improve the computational efficiency.

In the beginning, let us consider a $n$-dimensional problem. Table 1 presents the description of all parameters used in this problem.

Table 1: Description of all used parameters

| Notation | Designation | Dimension | Vector |
|---|---|---|---|
| $x$ | design variable vector | 1× n | $x_1, x_2, \ldots, x_n$ |
| $x_s$ | set of samples | n× 1 | $x_s = \{x^{(1)}, x^{(2)}, \ldots, x^{(n)}\}^T$ |
| $y_s$ | outputs responses of the samples set | n× 1 | $y_s = \{y^{(1)}, y^{(2)}, \ldots, y^{(n)}\}^T = \{y(x^{(1)}), y(x^{(2)}), \ldots, y(x^{(n)})\}^T$ |

The sampled data set is indicated by the pair $(x_s, y_s)$ in the vector space. The main aim of surrogate modeling is to build a meta-model in order to predict the output for any point $x$, thus, to estimate $y(x)$ based on the pair $(x_s, y_s)$.

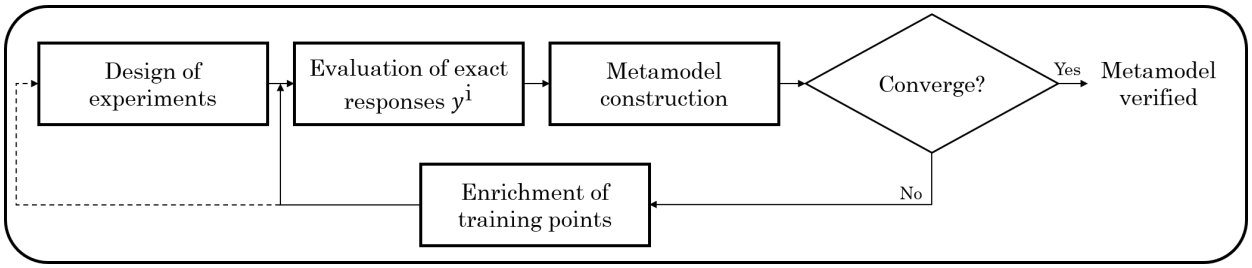


Figure 1: Surrogate modeling algorithm flowchart

The flowchart of the surrogate model process is presented in figure 1. Its implementation is a multi-step process. Forrester et al. [23] present some used techniques to solve this problem. First, Design Of Experiments (DOE) are applied by the surrogate modelling approach. Particulary, Latin Hypercube Sampling (LHS) [36] is used in order to repeat sampling in the design space. Kriging approach is then applied to represent the sampled data. Accordingly, surrogate model can replace the original analysis code during the RBDO procedure.

### *3.2. Kriging approach*

Nowadays, Kriging method is widely used as surrogate approach. In fact, it is characterized by its high quality of approximation with a required robustness, compared to other methods. Kriging method, also called Gaussian process modelling [37], consists of two nested functions:

a deterministic function $K(x)$ and a Gaussian random function $Z(x)$.
It can be written as follow:

$$y(x) = K(x) + Z(x) \tag{14}$$

$K(x)$ is usually determined as :

$$K(x) = \sum_{i=1}^{p-1} \boldsymbol{\beta_i} \boldsymbol{f_i}(x) \tag{15}$$

Here, $\boldsymbol{\beta} = [\beta_0, \beta_1, \ldots, \beta_{p-1}]^T$ and $f(x) = [f_0(x), f_1(x), \ldots, f_{p-1}(x)]^T$ present the regression coefficients vector and regression basis function vector respectively.
$Z(x)$ is a zero-mean stochastic process with a non-zero covariance given by:

$$Cov(Z(\mathbf{x}) - Z(\mathbf{x}')) = \sigma^2 R(\mathbf{x}, \mathbf{x}') \tag{16}$$

We note that $\sigma^2$ is the variance of $Z(x)$, $\mathbf{x}$ and $\mathbf{x}'$ are the estimated sampling points in the design space and $R(\mathbf{x}, \mathbf{x}')$ is the correlation function. It is an $m$-dimensional correlation functions constructed from *one*-dimensional correlation ones and obtained using a product correlation rule. For $m$ design variables, the correlation function is defined by:

$$R(\mathbf{x}, \mathbf{x}') = \prod_{i=1}^{m} R(x_i, x_i') \tag{17}$$

As mentioned in [38], exponential functions (equation (18)) and the Gaussian correlation functions (equation (19)) are the commonly used functions:

$$R(\mathbf{x}, \mathbf{x}') = \exp\left[-\sum_{i=1}^{m} \theta_i |x_i - x_i'|\right] \tag{18}$$

$$R(\mathbf{x}, \mathbf{x}') = \exp\left[-\sum_{i=1}^{m} \theta_i |x_i - x_i'|^2\right] \tag{19}$$

With, $\theta_i$ are the $m$-unknown parameters of $R(\mathbf{x}, \mathbf{x}')$. For any untried $\mathbf{x}$, the Kriging estimator [39] can be written as:

$$\hat{y}(\mathbf{x}) = \mathbf{r}^T(\mathbf{x})\mathbf{R}^{-1}(\mathbf{y}_S - \mathbf{F}^T\boldsymbol{\beta}) + \mathbf{f}^T(\mathbf{x})\boldsymbol{\beta} \tag{20}$$

$\hat{y}(\mathbf{x})$ is obtained by adding two functions. The first term consists in multiplying the untried sites correlation functions vector $\mathbf{r}(\mathbf{x}) = [R(\mathbf{x}, \mathbf{x}^{(1)}), R(\mathbf{x}, \mathbf{x}^{(2)}), \ldots, R(\mathbf{x}, \mathbf{x}^{(n)})]^T$ by the inverse of the correlation functions for the fitting sample matrix $\mathbf{R}$ and the vector of residuals for all fitting points $(\mathbf{y}_S - \mathbf{F}^T\boldsymbol{\beta})$. Here, $\mathbf{y}_S$ is the observed responses vector in the fitting sample and $\mathbf{F}$ is the model matrix of variable parameters. It can be presented by:

$$\boldsymbol{F} = \begin{bmatrix} 1 & x_1^{(1)} & \ldots & x_m^{(1)} & x_1^{(1)}x_2^{(1)} & \ldots & x_{m-1}^{(1)}x_m^{(1)} & (x_1^{(1)})^2 & \ldots & (x_m^{(1)})^2 \\ 1 & x_1^{(2)} & \ldots & x_m^{(2)} & x_1^{(2)}x_2^{(2)} & \ldots & x_{m-1}^{(1)}x_m^{(2)} & (x_1^{(2)})^2 & \ldots & (x_m^{(2)})^2 \\ \vdots & \vdots & \ddots & \vdots & \vdots & \ddots & \vdots & \vdots & \ddots & \vdots \\ 1 & x_1^{(n)} & \ldots & x_m^{(n)} & x_1^{(n)}x_2^{(n)} & \ldots & x_{m-1}^{(1)}x_m^{(n)} & (x_1^{(n)})^2 & \ldots & (x_m^{(n)})^2 \end{bmatrix} \tag{21}$$

The second term of (equation (20)) consists in multiplying the untired site regression basis function $\mathbf{f}^T(\mathbf{x})$ by the estimated regression coefficients vector $\boldsymbol{\beta}$.
Furthermore, the unknown model parameters $\boldsymbol{\beta}$, $\sigma^2$ and $\boldsymbol{\theta}$ presented in equations (15), (16), (18) and (19) respectively, needed to be determined to construct the Kriging predictor. To this end, a methodology based on the Gaussian process framework of Kriging approach is used. It consists in maximizing the likelihood function (equation (22)):

$$L(\boldsymbol{\beta}, \sigma^2, \boldsymbol{\theta}) = \frac{1}{\sqrt[n]{2\pi\sigma^2}\sqrt{|\mathbf{R}(\boldsymbol{\theta})|}} \exp\left[-\frac{(\mathbf{y}_S - \mathbf{F}^T\boldsymbol{\beta})^T\mathbf{R}^{-1}(\boldsymbol{\theta})(\mathbf{y}_S - \mathbf{F}^T\boldsymbol{\beta})}{2\sigma^2}\right] \tag{22}$$

To simplify this function, the natural logarithm is then applied to the likelihood expression:

$$\ln(L) = -\frac{n}{2}\ln(2\pi) - \frac{n}{2}\ln\left(\sigma^2\right) - \frac{1}{2}\ln(|\mathbf{R}(\boldsymbol{\theta})|) - \frac{(\mathbf{y}_S - \mathbf{F}^T\boldsymbol{\beta})^T\mathbf{R}^{-1}(\boldsymbol{\theta})(\mathbf{y}_S - \mathbf{F}^T\boldsymbol{\beta})}{2\sigma^2} \tag{23}$$

By canceling the derivative of equation (23) with respect to $\sigma^2$ and $\boldsymbol{\beta}$ we obtain the Maximum Likelihood Estimates (MLEs) $\hat{\boldsymbol{\beta}}$ and $\hat{\sigma}^2$:

$$\hat{\boldsymbol{\beta}} = \left(\mathbf{F}^T\mathbf{R}^{-1}\mathbf{F}\right)^{-1}\mathbf{F}^T\mathbf{R}^{-1}\mathbf{y}_S, \tag{24}$$

and

$$\hat{\sigma}^2 = \frac{(\mathbf{y}_S - \mathbf{F}^T\boldsymbol{\beta})^T\mathbf{R}^{-1}(\boldsymbol{\theta})(\mathbf{y}_S - \mathbf{F}^T\boldsymbol{\beta})}{n} \tag{25}$$

The estimator $\hat{\boldsymbol{\theta}}$ is obtained by solving the optimization problem of equation (26):

$$\begin{aligned} \max_{\theta} \quad & L(\boldsymbol{\theta}) = -\frac{1}{2}[n(\ln(2\pi) + \ln(\hat{\sigma}^2)) + \ln(|\mathbf{R}|)] \\ \text{s.t.} \quad & \theta_i > 0,\ i = 1, .., m \end{aligned} \tag{26}$$

After determining the estimator $\hat{\boldsymbol{\theta}}$ by solving equation (26), $\hat{\boldsymbol{\beta}}$ and $\hat{\sigma}^2$ can be defined using equations (24) and (25). Consequently, the prediction at any given point can be estimated by referring to equation (20).

### *3.3. Metamodel validation*

Referring to [40], the efficiency of the constructed surrogate model is influenced by the quantity and quality of the input dataset.

#### *3.3.1. Error measures*

To examine the efficiency of the constructed metamodel, the most simple way is to verify its residual errors. It consists in determining the difference between predicted response $\hat{y}^{(i)}$ and the original one $y^{(i)}$. Smaller residual error means grater estimator efficiency.
The most used error indicators of such a surrogate model are:

The Maximum Absolute Error (MAE):

$$MAE = \max \left| y^{(i)} - \hat{y}^{(i)} \right|, \quad i = 1, 2, ..., n_t \tag{27}$$

** The Relative Mean Error (RME):

$$RME = \frac{1}{n_t} \sum_{i=1}^{n_t} \left| \frac{y^{(i)} - \hat{y}^{(i)}}{y^{(i)}} \right| \tag{28}$$

*** The Root Mean Squared Error (RMSE):

$$RMSE = \sqrt{\frac{1}{n_t} \sum_{i=1}^{n_t} \left( y^{(i)} - \hat{y}^{(i)} \right)^2} \tag{29}$$

where $n_t$ is the sampling point number used to evaluate the error measures.

### *3.3.2. Cross validation*

The Cross-Validation (CV) is another error indicator which we can verify the accuracy of a surrogate model [41]. In CV, we define two type of samples data: training points responses $y^{(i)}$ and test points $\hat{y}_{-i}^{(i)}$ used to check its performances. It presents the prediction at $\mathbf{x}^{(i)}$ using the surrogate model constructed from all sampling points except $(\mathbf{x}^{(i)}, y^{(i)})$ [42]. The Mean Squares Error (generalized error) for 'leave-one-out CV' can then be defined as:

$$MSE_{CV} = \frac{1}{n} \sum_{i=1}^{n} \left( y^{(i)} - \hat{y}_{-i}^{(i)} \right)^2 \tag{30}$$

## 4. Multi-objective optimization study

### *4.1. Deterministic Multi-Objective Optimization problem (DMOO)*

Let's consider $M$ objective functions $f_m(x)$ to minimize. A DMOO approach is then required to minimize these functions considering geometrical, physical and functional constraints. Equation (31) can be then written as follow:

$$\begin{aligned} \min_{x} \quad & f_m(x), \quad m = 1, .., M \\ \text{s.t.} \quad & g_k(x) \leq 0, \quad k = 1, .., K \\ & h_j(x) = 0, \quad j = 1, .., J \\ & lb \leq x \leq ub \end{aligned} \tag{31}$$

Different from the mono-objective optimization, objective functions constitute a multi-dimensional space in the multi-objective optimization, called the *objective function space*, as well as the variable space used in all optimization problems. Figure 2 illustrates the transition from the design variable space to the objective function space. Furthermore, for each solution $x$, there is a point in the objective space, denoted by $(f_1, f_2, ..., f_M)^T$.

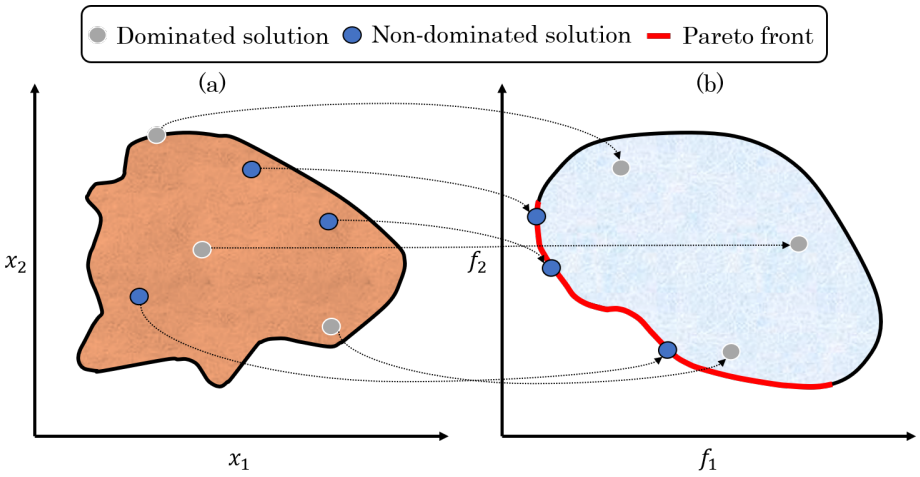


Figure 2: Transition from physical space (a) to objective space (b)

The DMOO approach aims to determine the optimal solution by choosing between a set of obtaining points on the Pareto front, using a higher-level qualitative considerations. Since, Evolutionary Multi-objective Optimization (EMO) approaches leads to find a set of non-dominated solutions by making each population of solutions in each iteration intuitive [43]. Figure 3 presents the EMO procedure for multi-objective optimization problems. It is based on two steps:

- Step1: consists in finding closest multiple non-dominated points to the Pareto-optimal front, with a wide trade-off among the objectives.
- Step2: consists in choosing the optimal point using higher-level information.

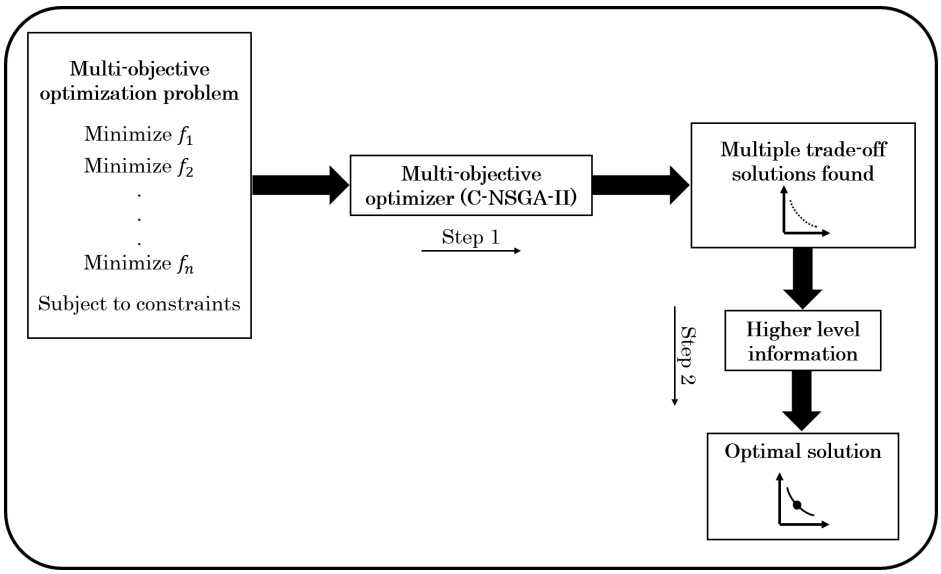


Figure 3: Flowchart of evolutionary multi-objective optimization procedure

### *4.2. Multi-objective reliability based-design optimization (MORBDO)*

Comparing with the DMOO, the MORBDO aims to find the best compromise between cost and reliability, taking into account design uncertainties. It can be mathematically presented by [44, 45]:

$$\begin{aligned} \min_{x} \quad & f_m(x), \quad m = 1, .., M \\ \text{s.t.} \quad & P_r[G_k(x, y) \leq 0] \leq P_k^T, \quad k = 1, .., K \\ & h_j(x) \leq 0, \quad j = 1, .., J \end{aligned} \tag{32}$$

$x$ and $y$ are deterministic and random variables respectively. $P_r[.]$ presents the probability operator and $P_i^T$ is the target failure probability. $h_j(x)$ and $G_i(x, y)$ are respectively the deterministic and the probabilistic constraints.

Dammak and El Hami [30] propose an efficient multi-objective optimization approach called MORBDO-HM. This method is based on the classical hybrid method proposed in [16, 17, 19]. The MORBDO-HM problem can be then described by:

$$\begin{aligned} \min_{x,y} \quad & F_m(x, y) = f_m(x) \times d_\beta(x, y), \quad m = 1, .., M \\ \text{s.t.} \quad & G(x, y) \leq 0 \\ & g_k(x, y) \leq 0, \quad k = 1, .., K \\ & d_\beta(x, y) \geq \beta_t \end{aligned} \tag{33}$$

It can be noted that $d_\beta$ is the distance between the most probable failure point and the optimal solution. It presents the reliability level and should be higher than the target reliability level $\beta_t$. It has been proved in [30] that, MORBDO-HM has efficiently provided an optimal solution where both physical and reliability constraints are respected. However, the optimization problem becomes more complex and it may converge to a non-feasible solution. To overcome this issue, an efficient method called MORBDO-RHM is proposed. The basic idea of this method is based on adding a new constraint to the optimization algorithm. The aim of this is to force the optimization problem to find the optimal point where both physical and reliability constraints are respected. Mathematically, it is defined as:

$$\begin{aligned} \min_{x,y} \quad & F(x, y) = f_m(x) \times d_\beta(x, y) \quad m = 1, .., M \\ \text{s.t.} \quad & G(x, y) \leq 0 \\ & g_k(x) \leq 0, \quad k = 1, .., K \\ & \beta(x, u) \geq \beta_t \\ & lb \leq x \leq ub \\ & f_m(x) \geq f_m(y) \end{aligned} \tag{34}$$

## 5. Numerical analysis

### *5.1. Description of the numerical model*

Figure 4 presents a three-dimensional model of the studied cooling system. It is composed by an aluminum heat sink which contains a $11 \times 12$ round pin fin matrix. Note that aluminum presents a high thermal conductivity as well as a lower mass (lower density). The dimensional details of the heat sink design are shown in figure 4.

The choice of this numerical configuration is based on an experimental study presented in [7]. The aim of this study is to propose a new methodology that leads to determine numerically an optimal design. To this end, firstly, this configuration needs to be validated with experimental data. Recently, several studies have been reported using metal-fins and metal-foam [46, 47]. However, the use of these configurations is limited to some specific applications and they are proportionally more expensive than classical ones.

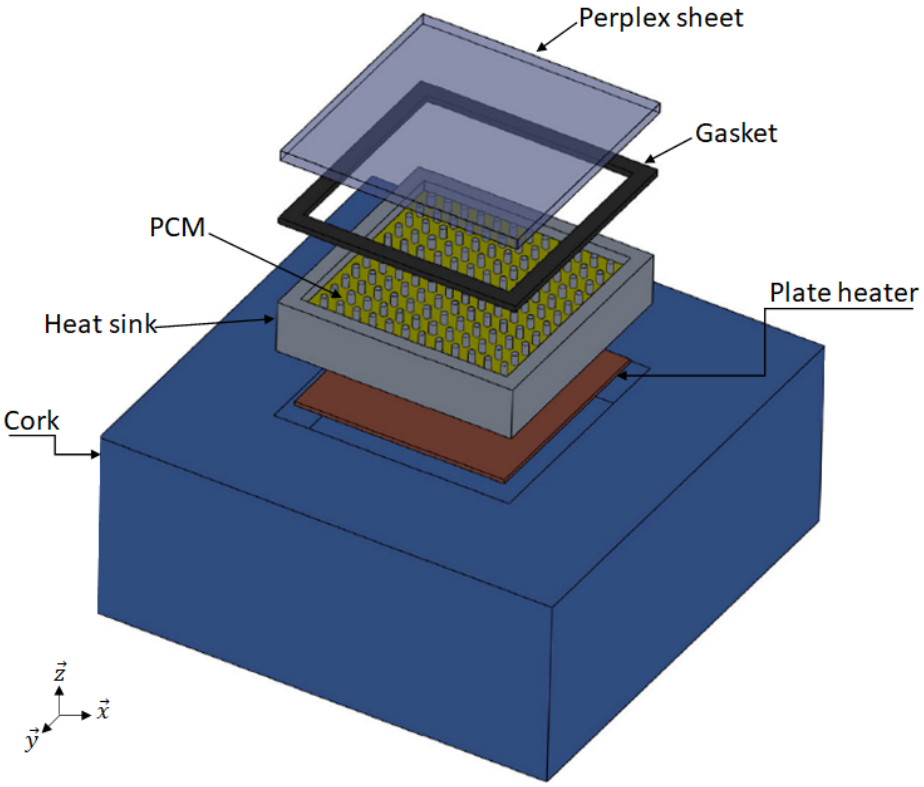


Figure 4: 3-D assembly of PCM-based heat sink

Experimentally, exterior walls of the heat sink are insulated with a rubber board, except the upper surface. The insulator presents a low thermal conductivity in order to minimize thermal losses and its properties are mentioned in table 2.

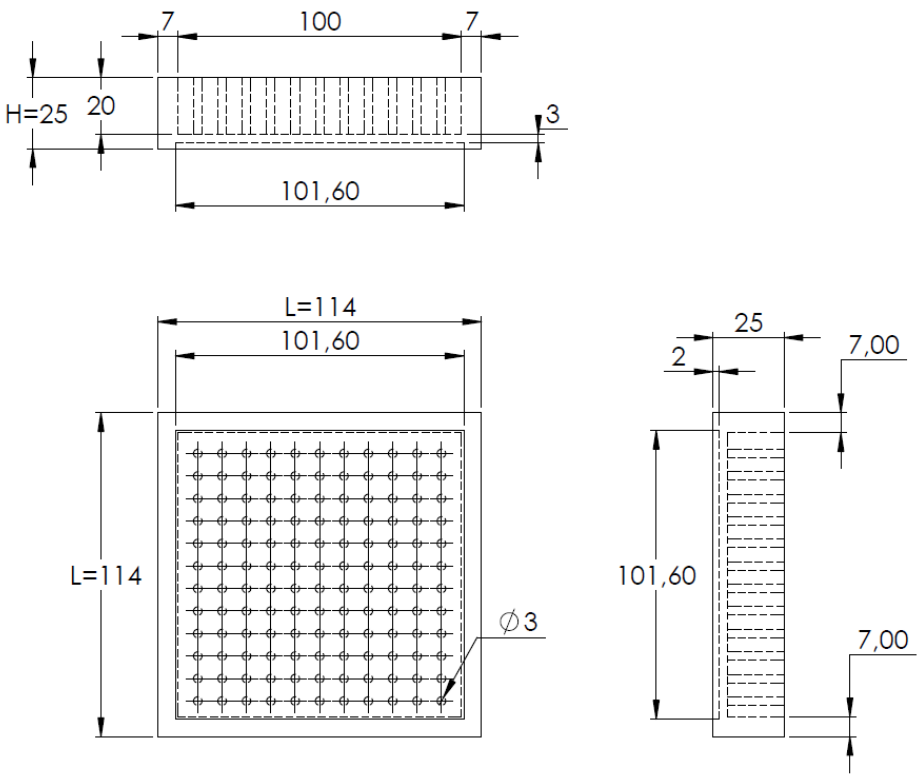


Figure 5: 2-D projections of 3mm round pin heat sink.

To control the liquid and solid fractions of PCM, the top surface is covered using silicon gasket and Perspex sheet. Note that these parts are not considered in the proposed numerical model.

The 3D numerical model is studied to compare the trends observed in the experimental results [7]. A uniform heat flux is supplied from the heat source to the bottom surface of the heat sink. It is transmitted then to the PCM, heat sink fins and finally to end walls. It can be considered that the model does not take into account marginal effects such as natural convection within melted PCM, and the volume changes in PCM after phase transition. All required material dimensions and thermo-physical properties of the studied system are available respectively in table 2 and table 3.

Table 2: Dimensions of required materials

| Material | Used materials | Dimensions |
|---|---|---|
| 1 | Perspex sheet | $115 \times 115 \times 5\ mm^3$ |
| 2 | Silicon rubber gasket | $115 \times 115 \times 5\ mm^3$ (with a cut out of $114 \times 114$) |
| 3 | Rubber pad for heat sink | $220 \times 220 \times 25\ mm^3$ (with a cut out of $114 \times 114$) |
| 4 | Rubber pad for heat sink bottom | $220 \times 220 \times 65\ mm^3$ |
| 5 | Plate heater | $101.6 \times 101.6 \times 2\ mm^3$ |

Table 3: Thermo-physical properties of each material

| Material | Thermal conductivity ($W/m.K$) | Specific heat ($kJ/kgK$) | Latent heat ($kJ/kg$) | Solidification point ($^{\circ}C$) | Melting point ($^{\circ}C$) | Density ($kg/m^3$) |
|---|---|---|---|---|---|---|
| Aluminum | 201 | 0.9 | - | - | 606.4 | 2700 |
| Paraffin Wax | 0.212(s) | 2.8(s) | 173.6 | 56 | 58 | 880(s) |
| | 0.167(l) | | | | | 790(l) |
| Rubber Pad | 0.043 | 1.23 | - | - | - | 2500 |

### *5.2. Boundary conditions*

A Finite Element (FE) computing software ANSYS Mechanical APDL is used to investigate the performance of the round pin fin heat sink filled with PCM.
A constant heat flux ($Q$=2800 $W/m^2$) is applied to mimic the heat source at the HS bottom (presented by the red plate in figure 4). The charging phase is established for 90$min$ and it is performed at room temperature of 18$^{\circ}C$.

The "enthalpy-porosity" approach is adopted in the PCM-based heat sink to investigate the effect of the transition phase. In this numerical investigation, several hypotheses are considered:

- The HS material is homogeneous and isotropic .
- A local thermal equilibrium between fins and liquid PCM is considered.
- Whatever the phase and the temperature, the thermo-physical properties of PCM and fins are considered constant .
- The radiative heat transfer is also neglected.

Natural convection is applied on exterior areas of the insulator. To deal with governing equations, initial conditions as well as applied boundary conditions are:

- Initial conditions:
  $t$=0, $T$=$T_{amb}$= 18$^{\circ}C$, $\xi$= 0.
  Otherwise, at t=0, global model is maintained at room conditions and the proposed PCM is totally in the solid phase.
- Heat flux applied at the HS base:

$$-\lambda \left.\frac{\partial T}{\partial x}\right|_{\substack{x=6.2\rightarrow 107.8\\ y=6.2\rightarrow 107.8\\ z=2}} = -\lambda \left.\frac{\partial T}{\partial y}\right|_{\substack{x=6.2\rightarrow 107.8\\ y=6.2\rightarrow 107.8\\ z=2}} = Q$$

### *5.3. Preliminary results and discussion*

Figure 6 shows the mesh of the global studied numerical design. It is divided into 39240 8-Node tetrahedral elements. Each element has eight nodes with a single degree of freedom,

temperature, at each node. It can be noted that a mesh refining is applied on the contact surfaces of HS and PCM to give a better result.

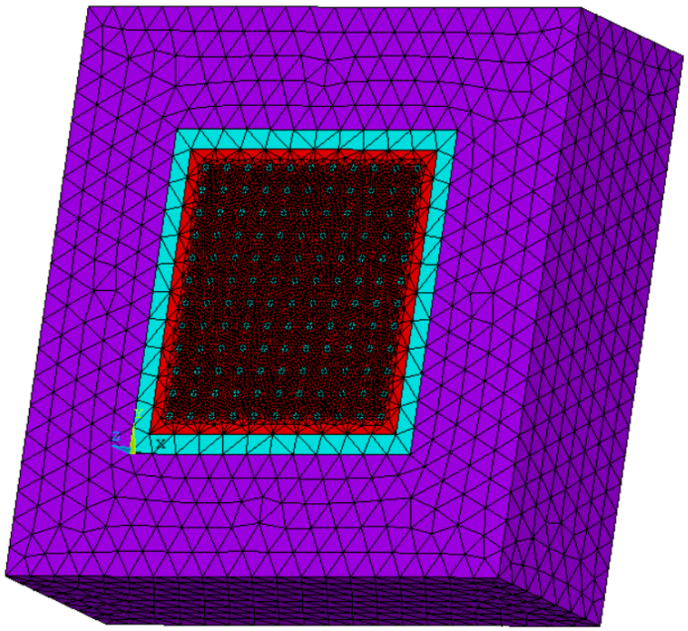

Figure 6: Mesh of studied model

Five different mesh sizes are investigated. The total computing time and the maximum reached temperature $T_{max}$ convergency are presented in table 4.

Table 4: Mesh convergency study

| Number of elements | 36240 | 38001 | 39240 | 85756 | 141367 |
|---|---|---|---|---|---|
| Simulation time $(min)$ | 11.55 | 12.7 | 12.87 | 27.5 | 85.15 |
| $T_{max}(°C)$ | 75.76 | 80.34 | 82.57 | 82.67 | 82.68 |

According to table 3, the mesh configuration with 39240 elements is chosen to compromise between cost and accuracy. In fact, the configuration with 141367 elements presents almost the same maximum reached temperature with a higher computing time comparing with 39240 elements configuration. Figure 7 presents the temperature-time profile at the HS base for 3 $mm$ pin fin heat sink configuration. Note that blue and red curves correspond respectively to experimental and numerical results during the charging phase under $Q$= 2800 $W/m^2$.

For the heating phase, the temperature variation profile can be discretized into three different regions:

- Solid region:
  Initially, the temperature increases in a linear way from the ambient temperature $T_{amb}$=18°C to the solidification temperature of PCM $T_s$=56°C.

- Liquid region:
  In this region, all the quantities of PCM inside enclosures will be totally melted. The temperature increases, until 90 $min$.

- Latent heating region:
  It can be seen that, for both numerical and experimental simulations, the increase of the temperature has been significantly delayed due to the use of PCM. In fact, benefiting from PCM thermo-physical properties, the energy generated by the input source is stored by the PCM and causes its transition from the solid phase to liquid phase.

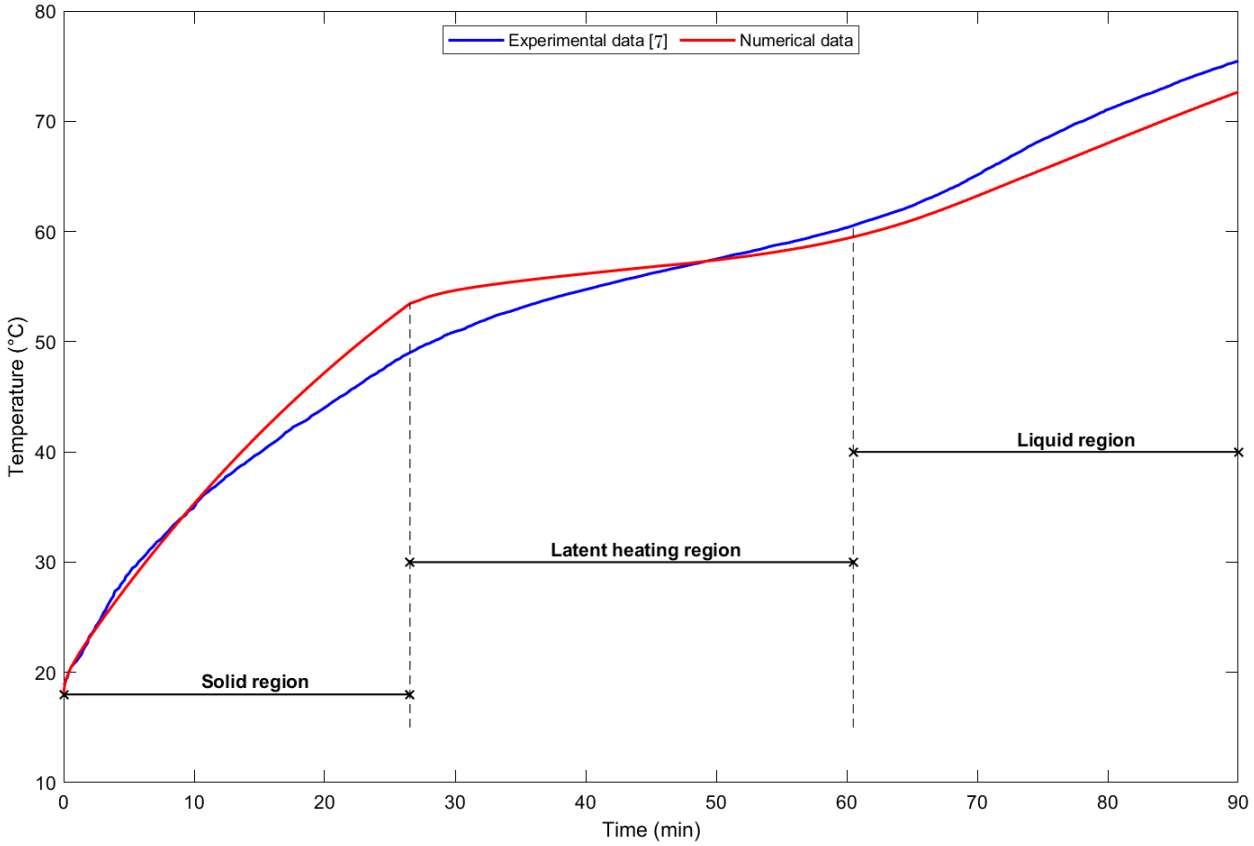


Figure 7: Temperature-time profile at the HS base under $Q$= 2800 $W/m^2$.

It can be observed that numerical data compare reasonably well with the experimental results found by Arshad et al. [7]. Hence, the coupled RBDO-metamodels problem can be then proceeded. The design parameters considered in this study are supposed a random probabilistic one which their characteristics are specified in table 5. We note that L and H are respectively the length and the height of the HS and $\phi$ is the pin-fin diameter (see figure 5).

In a mono-objective RBDO method, the aim is to minimize one objective function subject to physical and reliability constraint. For a PCM-based cooling system problem, the objective function is generally chosen as its total volume, considering the maximum reached temperature $T_{max}$. However, obtained optimal design may present several issues in term of heat dissipation for the discharging phase related to greater designs [11]. To overcome this problem, minimizing cooling time must be considered. We note by $t_f$ the final time to reach 25°C for the discharging phase. Furthermore, a 3D PCM-based heat sink model is expensive in term of computational time. Hence, the need to propose an original methodology of multiobjective RBDO coupled with surrogate model. Therefore, surrogate models are used to determine an approximation of $T_{max}$ and $t_f$ when changing design variables.

Table 5: Random variables properties

| Variables | Symbol | Distribution type | Cov | Mean value | Lower bound ($lb$) | Upper bound ($ub$) |
|---|---|---|---|---|---|---|
| Length ($mm$) | $L$ | Normal | 0.1 | 114 | 110 | 125 |
| Height ($mm$) | $H$ | Normal | 0.1 | 25 | 15 | 30 |
| Pin fin diameter ($mm$) | $\phi$ | Normal | 0.1 | 3 | 2 | 4 |

### *5.4. Surrogate model results: Kriging approach accuracy*

Meta-model approaches are applied to build estimations of the finite element simulation and determine the link between input parameters and their responses. The maximum reached temperature at the base of PCM-based round pin-fin heat sink is determined using Kriging surrogate models (equation (14)). To develop the Kriging meta-model, the Matlab toolbox package *Design and Analysis of Computer Experiments* (DACE) [48] is used. A second order polynomial global trend function and exponential correlation function are applied. Training data presented in (table 5) are then considered as the input of the FE analysis. The efficiency of the Kriging surrogate model is validated using error measures (equations (27) to (29)) as presented in table 6.

Table 6: Error measures of Kriging predictor

| Error measures | 20 LHS points | | 30 LHS points | | 50 LHS points | |
|---|---|---|---|---|---|---|
| | $T_{max}$ | $t_f$ | $T_{max}$ | $t_f$ | $T_{max}$ | $t_f$ |
| MAE | 1.354 | 2.054 | 1.216 | 2.1587 | 0.4353 | 1.3895 |
| RME | 1.046e-03 | 0.0032 | 8.1313e-04 | 0.0027 | 3.5979e-04 | 0.0017 |
| RMSE | 0.377 | 0.489 | 0.0905 | 0.7629 | 0.2531 | 0.3181 |

Training points number with LHS comparison is presented via the CV in figures 8 to 10 for 20, 30 and 50 LHS points, respectively.
It can be concluded that the Kriging model obtained by 50 LHS points gives an estimation of the original design with acceptable efficiency. In other words, the model validation using

the Kriging approach with 50 LHS points is more accurate than other configurations to estimate the link between input variables and their responses.

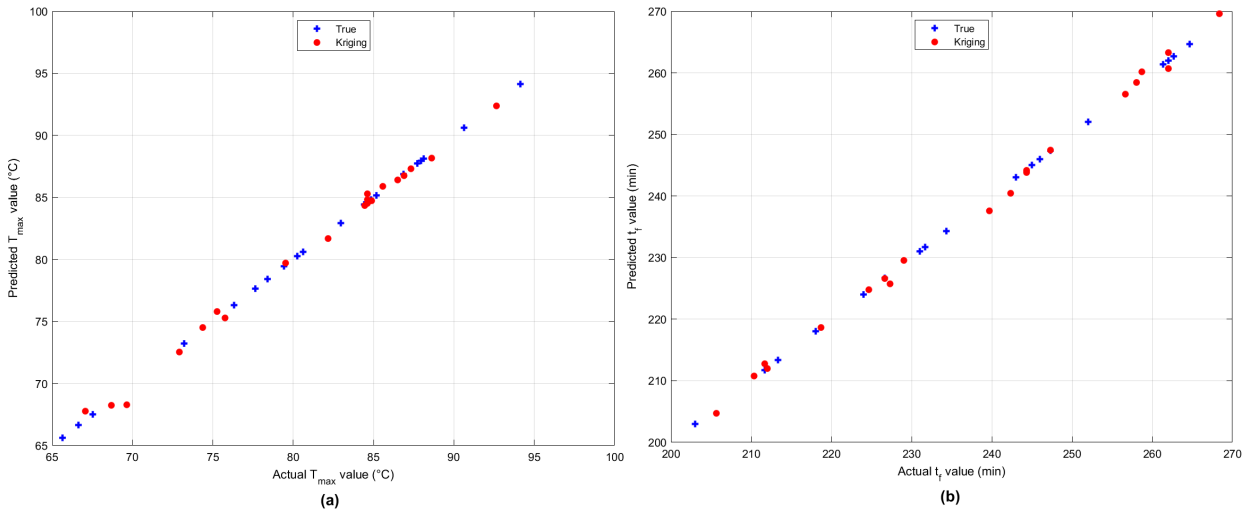


Figure 8: Cross-validation using Kriging predictor with 20 LHS points for (a) $T_{max}$ and (b) $t_f$

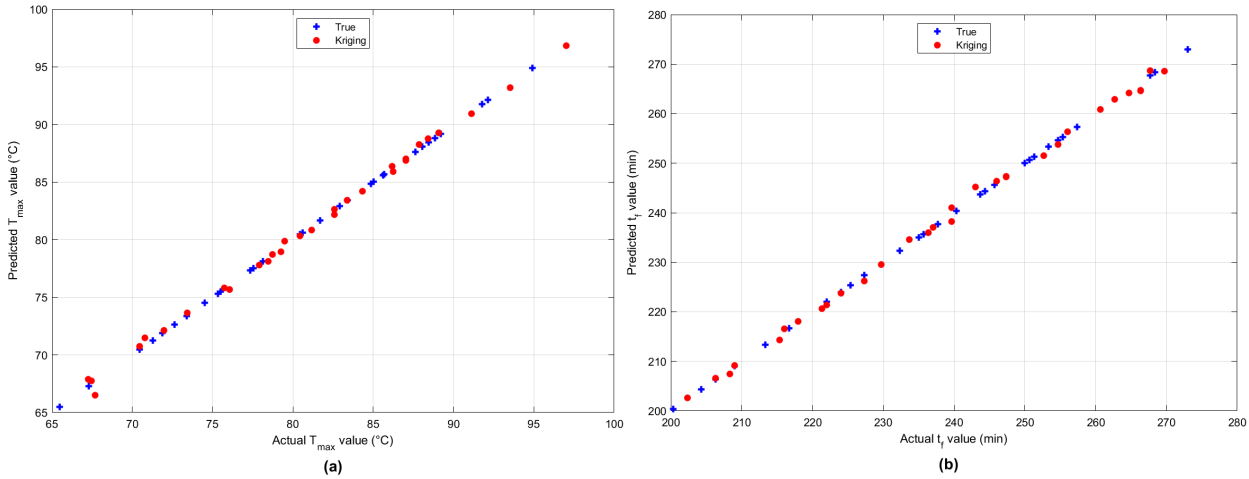


Figure 9: Cross-validation using Kriging predictor with 30 LHS points for (a) $T_{max}$ and (b) $t_f$

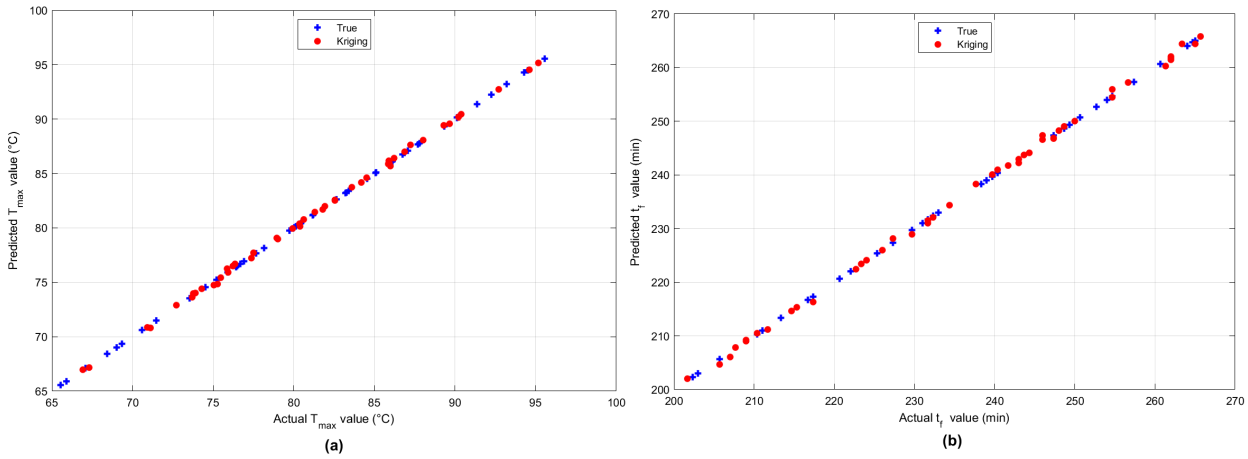


Figure 10: Cross-validation using Kriging predictor with 50 LHS points for (a) $T_{max}$ and (b) $t_f$

In the next section, Kriging model will be coupled with MORBDO simulation to analyze optimization and reliability of the studied system.

### *5.5. MORBDO for PCM-based heat sink*

In [49], authors develop the constrained non-dominated sorting genetic algorithm (C-NSGA-II) to solve the optimization problem.
Pareto front using different populations sizes comparison is presented in figure 11. In this paper, a maximum of 500 generations and a population size of 200 are used. This configuration is used in order to determine if the spread in solutions is maintained.

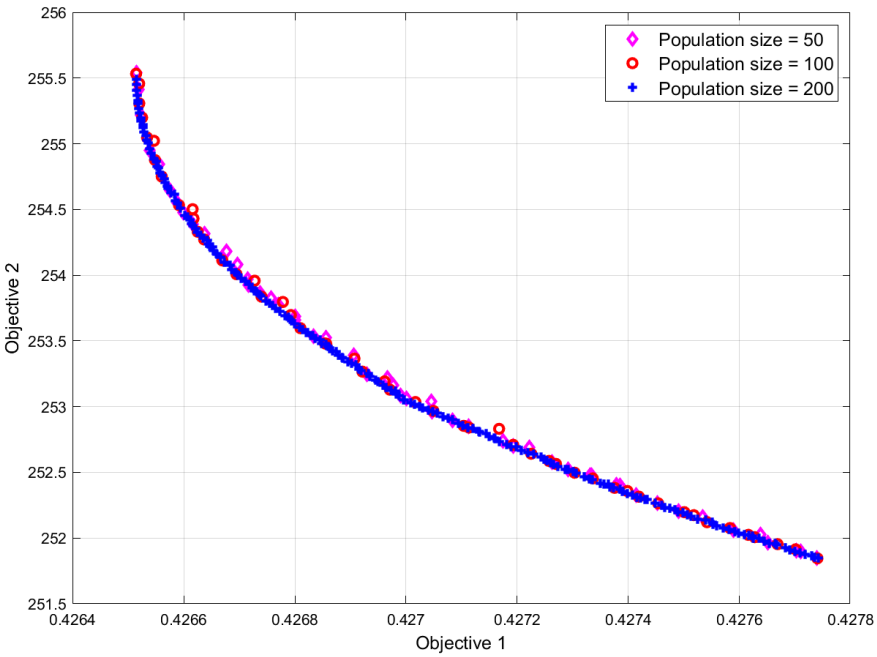


Figure 11: A comparison between different populations sizes

The optimization problem is based on minimizing the cooling system volume as well as the final time ($t_f$) taken for the discharging phase subject to the maximum reached temperature ($T_{max}$). Note that the critical temperature for the charging phase is about $T_{crit} = 70°C$. Generally, the target reliability level is supposed equal to: $\beta_t$=3 which corresponds to a failure probability about $10^{-3}$.

### *5.5.1. Results of DMOO*

For the DMOO approach, the global safety factor $S_g$ is chosen based on engineering experience. Consequently, the optimal design temperature should be lower than the critical values. Then, the DMOO problem is defined as:

$$\begin{aligned} \min_{x} \quad & \{f_1(x) = V, f_2(x) = t_f\} \\ \text{s.t.} \quad & T_{max}(x) \leq \frac{T_{crit}}{S_g} \\ & lb \leq x \leq ub \end{aligned} \tag{35}$$

Figure 12 presents the Pareto optimal front of DMOO. It provides, for design selection, decision-makers with a set of solutions over the Pareto space. To select the best optimum, called knee point [50], the Minimum Distance Selection Method (MDSM) [51] is considered here as shown in figure 12. In a Pareto front, the knee point provides a good trade-off between the objective functions. It presents the minimal distance from the utopia point.

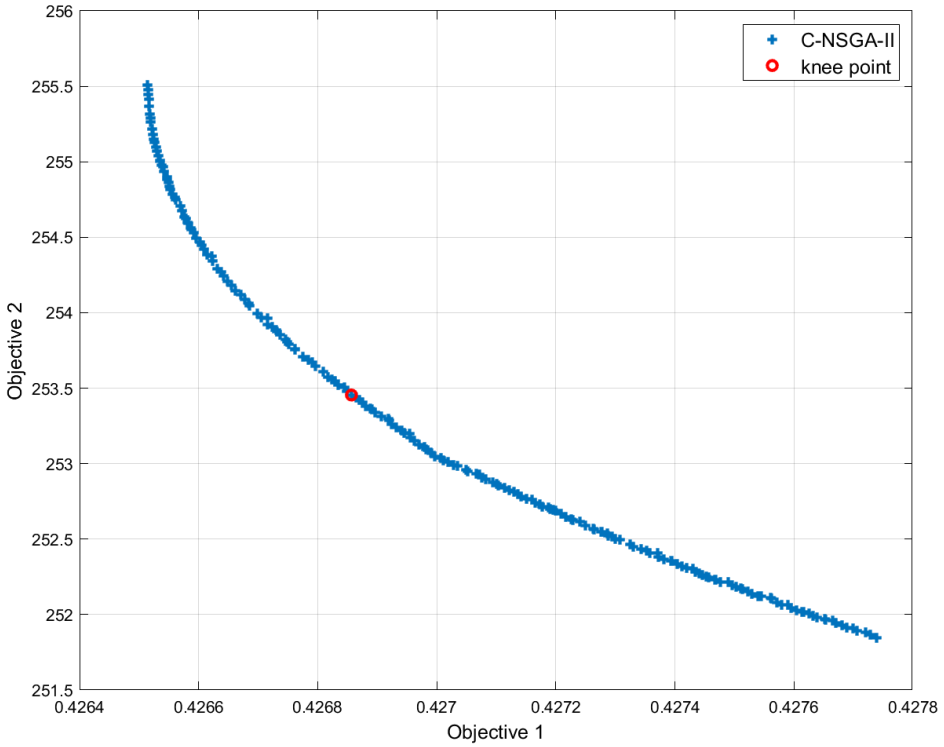


Figure 12: DMOO Pareto front

Table 7 presents the deterministic MOO results. Referring to the baseline model, the DMOO approach presents an optimal design (the thermal constraint is verified), but its reliability level $\beta$ is missing ($\beta$=1.85<3). Therefore, to solve this issue, MORBDO methods are extremely recommended.

Table 7: DMOO results

| Description | | Design point $y^*$ | Optimal solution $x^*$ |
|---|---|---|---|
| Design variables | $L\ (mm)$ | 125 | 125 |
| | $H\ (mm)$ | 23.78 | 28.64 |
| | $\phi\ (mm)$ | 4 | 3.72 |
| Objective function | $V\ (mm^3)$ | 3.51e+05 | 4.268e+05 |
| | $t_f\ (min)$ | 236.47 | 253.45 |
| Thermal constraint | $T_{max}\ (°C)$ | 70 | 63 |
| Reliability value | $\beta$ | | 1.85 |

### *5.5.2. Results of MORBDO*

Equation (36) and equation (37) present respectively the MORBDO-HM and MORBDO-RHM optimization problem:

$$\begin{aligned} \min_{x,y} \quad & F(x,y) = [V(x), t_f(x)] \times d_\beta(x,y) \\ \text{s.t.} \quad & T_{max}(y) \leq 70°C \\ & lb \leq x, y \leq ub \\ & d_\beta(x,y) \geq \beta_t \end{aligned} \tag{36}$$

$$\begin{aligned} \min_{x,y} \quad & F(x,y) = [V(x), t_f(x)] \times d_\beta(x,y) \\ \text{s.t.} \quad & T_{max}(y) \leq 70°C \\ & lb \leq x, y \leq ub \\ & d_\beta(x,y) \geq \beta_t \\ & V(x) \geq V(y) \\ & t_f(x) \geq t_f(y) \end{aligned} \tag{37}$$

The corresponding Pareto front is illustrated in figure 13 for both MORBDO-HM and MORBDO-RHM. MORBDO results are presented in table 8. As well as DMOO, MORBDO results provide a set of optimal points over the Pareto space. Against DMOO, the reliability level with MORBDO is respected.

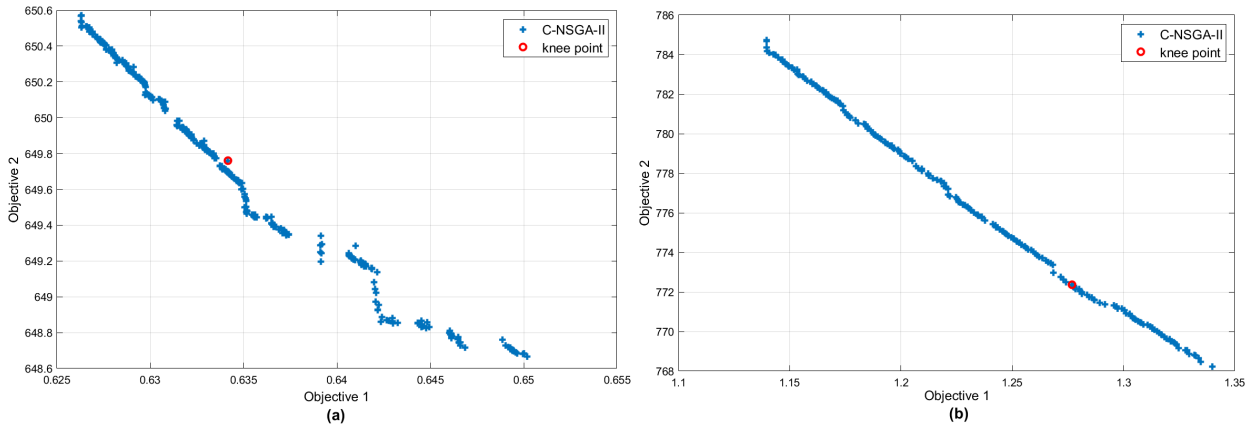


Figure 13: Pareto optimal front: (a) MORBDO-HM and (b) MORBDO-RHM

Table 8 illustrated that MORBDO-HM gives an optimal resulted point within the failure zone ($T_{max} = 90.98°C$ >70°C). However, the MORBDO-RHM leads to obtain an optimal configuration with respect of reliability constraint as well as thermal constraint, comparing with DMOO and MORBDO-HM approaches.

Table 8: MORBDO results

| Descrption | | MORBDO-HM | | MORBDO-RHM | |
|---|---|---|---|---|---|
| | | Design point $y^*$ | Optimal solution $x^*$ | Design point $y^*$ | Optimal solution $x^*$ |
| Design variables | $L(mm)$ | 124.67 | 110.81 | 122.62 | 121.96 |
| | $H(mm)$ | 24.04 | 18.89 | 26.82 | 30 |
| | $\phi(mm)$ | 4 | 4 | 2.82 | 3.92 |
| Objective functions | $V(mm^3)$ | 3.53e+05 | 2.11e+05 | 3.8279e+05 | 4.2558e+05 |
| | $t_f(min))$ | 237.43 | 216.56 | 254.8 | 257.42 |
| Thermal constraint | $T_{max}°C)$ | 70 | 90.98 | 69.86 | 64.61 |
| Reliability value | $\beta$ | | 3 | | 3 |

The temperature-time profile, measured at the HS base, is presented in figure 14, for baseline design (red curve) and MORBDO-RHM design (blue curve). In this figure, charging and discharging phases of cooling electronic devices are investigated.

As presented in figure 14 and table 8, the optimal design obtained by the MORBDO-RHM approach verifies both thermal and reliability constraints. In fact, at $t = 120min$, the maximum reached temperature $T_{max}$ is lower than the critical temperature, which guarantees a better performance of the electronic component. Moreover, reliability condition is verified with this model. In fact, the reliability level of the optimal design is equal to the target reliability level ($\beta_{MORBDO-RHM} \geq \beta_t$). However, the baseline model does not respect this condition and it may lead to an immediate failure of the electronic component. Furthermore, for the optimal configuration, the latent heating phase period is more important than its for baseline design throughout the charging phase. This can be explained by the fact that

the optimal configuration has the ability to store a large amount of thermal energy against the baseline design. On the other hand, for the discharging phase, optimal design has the ability to release the stored thermal energy in a minimal time compared with initial model. In fact, PCM takes about $40min$ to reach its solid states against over than $55min$ for the initial model.

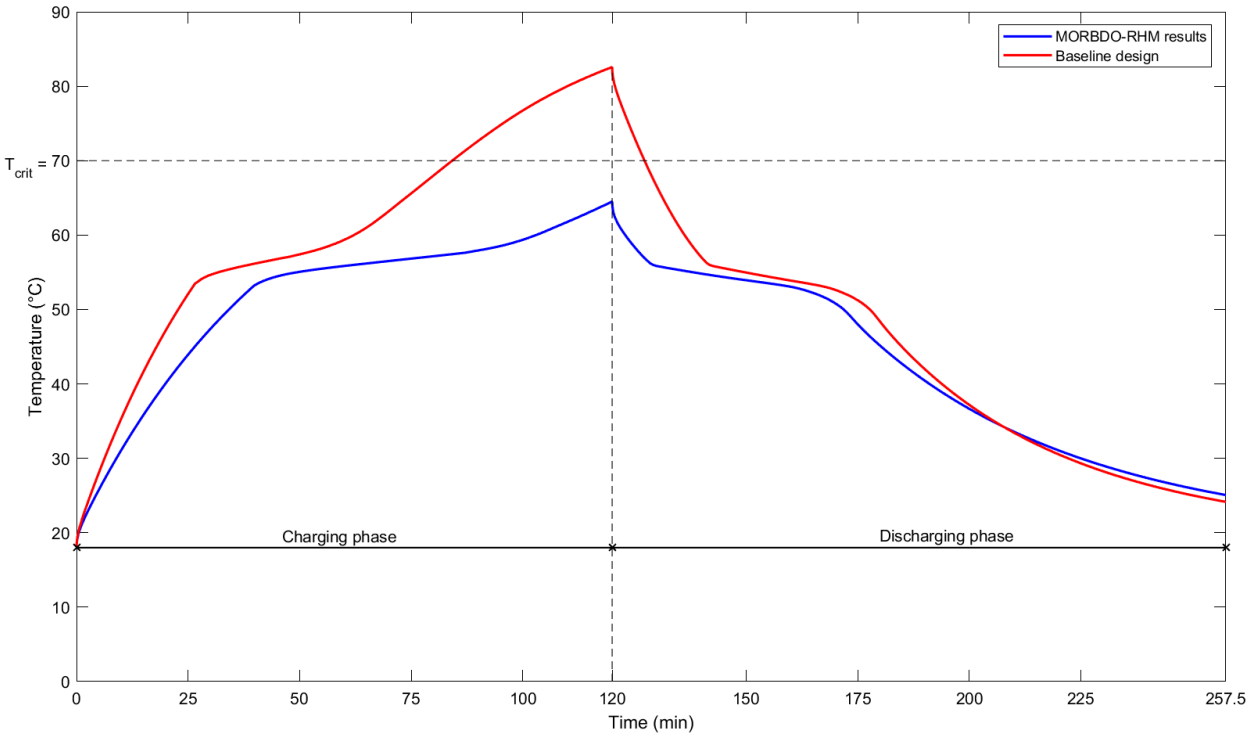


Figure 14: Temperature profile for baseline design and optimal design: charging and discharging phases.

## 6. Conclusion

This paper aims to propose an efficient method that leads to obtain an optimal configuration of thermal management systems based on PCM technology which ensure a recommended reliability level. In this work, a 3D transient numerical simulation of round pin-fin heat sink fully filled with PCM is studied to investigate the thermal management behaviours for passive cooling of electronic equipments.

Experimental results founded by Arshad et al. [7] are numerically validated for PCM embedded in $3mm$ round pin fin heat sink configuration subject to constant heat load (about 2800 $W/m^2$).

To determine the relationship between the input and output variables, Kriging approach is used in the construction of the surrogate model. The results of cross-validation and error measures show that Kriging estimator with 50 LHS points gives an approximation of the original design with great accuracy.

Although the DMOO approach is easy to apply and can ensure an optimum design, a reliability level of thermal constraint is missed. Therefore, and in order to overcome this

issue, MORBDO methods are investigated for thermal management applications. MORBDO-RHM and MORBDO-HM approaches based on surrogate models are coupled with PCM-based heat sink design.

The numerical study proves that the proposed MORBDO-RHM approach is more efficient and reliable comparing with MORBDO-HM approach. We conclude that, for thermal enhancer application using PCM-based HS, MORBDO-RHM approach leads to obtain an optimal design, where both thermal and reliability constraints are verified. The proposed methodology can be then applied to determine an optimal design of cooling systems that guarantees a higher performance of electronic components. Furthermore, it gives a better compromise between safety and cost, for both charging and discharging phases. An extension to other heat sink configurations such as square and triangular pin-fin heat sink needs to be studied and validated with experimental investigation.

## References


[1] Ravi Kandasamy, Xiang-Qi Wang, and Arun S Mujumdar. Transient cooling of electronics using phase change material (pcm)-based heat sinks. *Applied thermal engineering*, 28(8-9):1047–1057, 2008.

[2] Akın Burak Etemoglu. A brief survey and economical analysis of air cooling for electronic equipments. *International communications in heat and mass transfer*, 34(1):103–113, 2007.

[3] Ronan Grimes, Ed Walsh, and Pat Walsh. Active cooling of a mobile phone handset. *Applied Thermal Engineering*, 30(16):2363–2369, 2010.

[4] Zhaoxia Luo, Hyejung Cho, Xiaobing Luo, and Kyung-il Cho. System thermal analysis for mobile phone. *Applied Thermal Engineering*, 28(14-15):1889–1895, 2008.

[5] Rajesh Baby and C Balaji. Thermal performance of a pcm heat sink under different heat loads: an experimental study. *International Journal of Thermal Sciences*, 79:240–249, 2014.

[6] Ibrahim Mjallal, Hussien Farhat, Mohammad Hammoud, Samer Ali, and Ibrahim Assi. Improving the cooling efficiency of heat sinks through the use of different types of phase change materials. *Technologies*, 6(1):5, 2018.

[7] Adeel Arshad, Hafiz Muhammad Ali, Shahab Khushnood, and Mark Jabbal. Experimental investigation of pcm based round pin-fin heat sinks for thermal management of electronics: effect of pin-fin diameter. *International Journal of Heat and Mass Transfer*, 117:861–872, 2018.

[8] Jesto Thomas, PVSS Srivatsa, S Ramesh Krishnan, and Rajesh Baby. Thermal performance evaluation of a phase change material based heat sink: A numerical study. *Procedia technology*, 25:1182–1190, 2016.

[9] Bessem Debich, Abdelkhalak El Hami, Ahmed Yaich, Wajih Gafsi, Lassaad Walha, and Mohamed Haddar. Design optimization of pcm-based finned heat sinks for mechatronic components: A numerical investigation and parametric study. *Journal of Energy Storage*, 32:101960, 2020.

[10] Abdelkhalak El Hami and Radi Bouchaib. *Uncertainty and optimization in structural mechanics*. Wiley Online Library, 2013.

[11] Bessem Debich, Abdelkhalak El Hami, Ahmed Yaich, Wajih Gafsi, Lassaad Walha, and Mohamed Haddar. An efficient reliability-based design optimization study for pcm-based heat-sink used for cooling electronic devices. *Mechanics of Advanced Materials and Structures*, pages 1–13, 2020.

[12] Bessem Debich, Ahmed Yaich, Abdelkhalak Elhami, Wajih Gafsi, Lassaad Walha, and Mohamed Haddar. Coupling pcm-based heat sinks finite elements model for mechatronic devices with design optimization procedure. In *2020 IEEE 6th International Conference on Optimization and Applications (ICOA)*, pages 1–4. IEEE, 2020.

[13] A Makhloufi, Y Aoues, and A El Hami. Reliability based design optimization of wire bonding in power microelectronic devices. *Microsystem Technologies*, 22(12):2737–2748, 2016.

[14] A El Hami and Bouchaib Radi. Comparison study of different reliability-based design optimization approaches. In *Advanced materials research*, volume 274, pages 113–121. Trans Tech Publ, 2011.

[15] A Abo Al-Kheer, Abdelkhalak El-Hami, Mohamed Ghias Kharmanda, and Abdel Mouem Mouazen. Reliability-based design for soil tillage machines. *Journal of Terramechanics*, 48(1):57–64, 2011.

[16] G Kharmanda, A Mohamed, and Maurice Lemaire. Efficient reliability-based design optimization using a hybrid space with application to finite element analysis. *Structural and Multidisciplinary Optimization*, 24(3):233–245, 2002.

[17] A Yaich, G Kharmanda, Abdelkhalak El Hami, L Walha, and M Haddar. Reliability based design optimization for multiaxial fatigue damage analysis using robust hybrid method. *Journal of Mechanics*, 34(5):551–566, 2018.

[18] K Dammak, A El Hami, S Koubaa, L Walha, and M Haddar. Reliability based design optimization of coupled acoustic-structure system using generalized polynomial chaos. *International Journal of Mechanical Sciences*, 134:75–84, 2017.

[19] Khalil Dammak, Ahmed Yaich, Abdelkhalak El Hami, Lassaad Walha, and Mohamed Haddar. An efficient optimization based on the robust hybrid method for the coupled acoustic–structural system. *Mechanics of Advanced Materials and Structures*, pages 1–11, 2018.

[20] Fatma Abid, Abdelkhalak El Hami, Tarek Merzouki, Lassaad Walha, and Mohamed Haddar. An approach for the reliability-based design optimization of shape memory alloy structure. *Mechanics Based Design of Structures and Machines*, pages 1–17, 2019.

[21] A Kamel, K Dammak, A El Hami, M Ben Jdidia, L Hammami, and M Haddar. A modified hybrid method for a reliability-based design optimization applied to an offshore wind turbine. *Mechanics of Advanced Materials and Structures*, pages 1–14, 2020.

[22] Ahmed Yaich, Fatma Abid, Tarek Merzouki, Abdelkhalak El Hami, Lassaad Walha, and Mohamed Haddar. A robust method for the reliability-based design optimization of shape memory alloy actuator. *Mechanics Based Design of Structures and Machines*, pages 1–19, 2021.

[23] Alexander Forrester, Andras Sobester, and Andy Keane. *Engineering design via surrogate modelling: a practical guide*. John Wiley & Sons, 2008.

[24] Achille Messac. *Optimization in practice with MATLAB®: for engineering students and professionals*. Cambridge University Press, 2015.

[25] A Ben Abdessalem and Abdelkhalak El-Hami. A probabilistic approach for optimising hydroformed structures using local surrogate models to control failures. *International Journal of Mechanical Sciences*, 96:143–162, 2015.

[26] K Dammak, S Koubaa, A El Hami, L Walha, and M Haddar. Numerical modelling of vibro-acoustic problem in presence of uncertainty: Application to a vehicle cabin. *Applied Acoustics*, 144:113–123, 2019.

[27] A Guerine, A El Hami, L Walha, T Fakhfakh, and M Haddar. A polynomial chaos method for the analysis of the dynamic behavior of uncertain gear friction system. *European Journal of Mechanics-A/Solids*, 59:76–84, 2016.

[28] Changwu Huang, Bouchaïb Radi, and Abdelkhalak El Hami. Uncertainty analysis of deep drawing using surrogate model based probabilistic method. *The International Journal of Advanced Manufacturing Technology*, 86(9-12):3229–3240, 2016.

[29] Fatma Abid, Khalil Dammak, Abdelkhalak El Hami, Tarek Merzouki, Hassen Trabelsi, Lassaad Walha, and Mohamed Haddar. Surrogate models for uncertainty analysis of micro-actuator. *Microsystem Technologies*, pages 1–12, 2020.

[30] Khalil Dammak and Abdelkhalak El Hami. Multi-objective reliability based design optimization using kriging surrogate model for cementless hip prosthesis. *Computer Methods in Biomechanics and Biomedical Engineering*, pages 1–14, 2020.

[31] Khalil Dammak and Abdelkhalak El Hami. Multi-objective reliability based design optimization of coupled acoustic-structural system. *Engineering Structures*, 197:109389, 2019.

[32] Yue-Tzu Yang and Yi-Hsien Wang. Numerical simulation of three-dimensional transient cooling application on a portable electronic device using phase change material. *International Journal of*

*Thermal Sciences*, 51:155 – 162, 2012.

[33] Yi-Hsien Wang and Yue-Tzu Yang. Three-dimensional transient cooling simulations of a portable electronic device using pcm (phase change materials) in multi-fin heat sink. *Energy*, 36(8):5214 – 5224, 2011. PRES 2010.

[34] V. Shatikian, G. Ziskind, and R. Letan. Numerical investigation of a pcm-based heat sink with internal fins: Constant heat flux. *International Journal of Heat and Mass Transfer*, 51(5):1488 – 1493, 2008.

[35] K.C. Nayak, S.K. Saha, K. Srinivasan, and P. Dutta. A numerical model for heat sinks with phase change materials and thermal conductivity enhancers. *International Journal of Heat and Mass Transfer*, 49(11):1833 – 1844, 2006.

[36] Michael D McKay, Richard J Beckman, and William J Conover. A comparison of three methods for selecting values of input variables in the analysis of output from a computer code. *Technometrics*, 42(1):55–61, 2000.

[37] Christopher KI Williams and Carl Edward Rasmussen. *Gaussian processes for machine learning*, volume 2. MIT press Cambridge, MA, 2006.

[38] Tushar Goel, Willem Roux, and Nielen Stander. A topology optimization tool for ls-dyna users: Ls-opt/topology. In *7th european LS-Dyna conference*, pages 14–15, 2009.

[39] Bilal M Ayyub and George J Klir. *Uncertainty modeling and analysis in engineering and the sciences*. CRC Press, 2006.

[40] Ann-Britt Ryberg, Rebecka Domeij Bäckryd, and Larsgunnar Nilsson. *Metamodel-based multidisciplinary design optimization for automotive applications*. Linköping University Electronic Press, 2012.

[41] Martin Meckesheimer, Andrew J Booker, Russell R Barton, and Timothy W Simpson. Computationally inexpensive metamodel assessment strategies. *AIAA journal*, 40(10):2053–2060, 2002.

[42] Alexander IJ Forrester and Andy J Keane. Recent advances in surrogate-based optimization. *Progress in aerospace sciences*, 45(1-3):50–79, 2009.

[43] Kalyanmoy Deb. Multi-objective optimisation using evolutionary algorithms: an introduction. In *Multi-objective evolutionary optimisation for product design and manufacturing*, pages 3–34. Springer, 2011.

[44] A Elhami, G Lallement, P Minotti, and S Cogan. Methods that combine finite group theory with component mode synthesis in the analysis of repetitive structures. *Computers & structures*, 48(6):975–982, 1993.

[45] Jianguang Fang, Yunkai Gao, Guangyong Sun, and Qing Li. Multiobjective reliability-based optimization for design of a vehicledoor. *Finite Elements in Analysis and Design*, 67:13–21, 2013.

[46] Mohamed Moussa El Idi and Mustapha Karkri. Heating and cooling conditions effects on the kinetic of phase change of pcm embedded in metal foam. *Case Studies in Thermal Engineering*, 21:100716, 2020.

[47] Mohamed Moussa El Idi and Moustapha Karkri. Melting and solidification behavior of pcm embedded in metal foam. In *COMSOL CONFERENCE 2020 EUROPE*, 2020.

[48] Søren Nymand Lophaven, Hans Bruun Nielsen, Jacob Søndergaard, et al. *DACE: a Matlab kriging toolbox*, volume 2. Citeseer, 2002.

[49] Kalyanmoy Deb, Amrit Pratap, Sameer Agarwal, and TAMT Meyarivan. A fast and elitist multiobjective genetic algorithm: Nsga-ii. *IEEE transactions on evolutionary computation*, 6(2):182–197, 2002.

[50] Guangyong Sun, Guangyao Li, Shiwei Zhou, Hongzhou Li, Shujuan Hou, and Qing Li. Crashworthiness design of vehicle by using multiobjective robust optimization. *Structural and Multidisciplinary Optimization*, 44(1):99–110, 2011.

[51] Samer Barakat, Khaldoon Bani-Hani, and Mohammed Q Taha. Multi-objective reliability-based optimization of prestressed concrete beams. *Structural Safety*, 26(3):311–342, 2004.